Journal of Materials Chemistry B

ROYAL SOCIETY OF CHEMISTRY

PAPER

View Article Online
View Journal | View Issue

Check for updates

Cite this: J. Mater. Chem. B, 2026, 14, 4426

Fibroin/sulfated alginate membranes containing exosomes of stem cells treated with B and Zn-doped hydroxyapatite for periosteal tissue engineering

Sema Akbaba, [ab] Senem Ozge Turacli Karaguven, [c] Zafer Evis [d] and Ayşen Tezcaner *[ade]

Received 11th December 2025,
Accepted 8th March 2026

DOI: 10.1039/d5tb02784e

rsc.li/materials-b

Periosteal regeneration requires tissue engineering strategies that simultaneously support osteogenesis, angiogenesis, and immunomodulation. In this study, fibroin/sulfated alginate (F/sA) composite membranes loaded with exosomes derived from human adipose-derived stem cells (hADSCs) treated with pure, 4 mol% B-doped, and 4 mol% B and 8 mol% Zn-doped hydroxyapatite (HA) were developed for periosteal tissue engineering. It was hypothesized that incorporation of sA and HA-conditioned exosomes enhances osteoimmunomodulation while preserving scaffold integrity. F/sA membranes with varying sulfated alginate content (0–20 wt%) were fabricated and characterized. Increasing sulfated alginate content enhanced water uptake and degradation while reducing tensile strength and Young's modulus. A 95 : 5 F/sA ratio was identified as optimal exosome delivery composition, exhibiting the highest hADSC viability and reducing IL1B and CASP1 levels in THP-1 macrophages ($p < 0.05$). It was also found that exosomes isolated from pure and doped HA-treated hADSCs showed treatment-dependent alterations in the cargo. The 8 mol% B-doped HA group significantly increased exosome yield, while all HA treatments reduced protein/particle and DNA/particle ratios. Doped HA treatments significantly increased RNA/particle ratio ($p < 0.05$). Exosome-loaded F/sA membranes enhanced early cell attachment and proliferation and significantly promoted osteogenic differentiation of hADSCs, increasing *RUNX2*, *COL1A1*, and *OCN* expression. Immunomodulatory effects were observed for all exosome groups, except for the 4 mol% B and 8 mol% Zn-doped HA groups, which significantly increased *CASP1* expression. Overall, this study demonstrates that HA doping modulates exosomal composition in a dopant-dependent manner and that exosome-functionalized F/sA membranes constitute a multifunctional periosteal substitute with tunable properties.

1. Introduction

Periosteum is the substantial membrane enclosing bones.[1] Periosteum houses fibroblasts, osteoblasts, bone precursor cells and stem cells, playing a crucial role in both embryonic osteogenesis and bone defect repair.[2,3] In case of damage, stem cells present in periosteum ensure bone regeneration by migrating towards the defect area and modulate inflammation in a cross-talk with macrophages.[4,5] Periosteum is also a highly vascularized tissue, which enables nutrient transport needed for bone maintenance and regeneration.[3] Open fractures and tumor curettages damage periosteum, which impairs healing.[6] Periosteum's importance in bone regeneration led to research on its regeneration. In a study, decellularized pig periosteum was shown to increase M2 polarization of macrophages in a rat cranial critical-size defect model.[7] However, it was also stated that the dense fibrous structure of decellularized periosteum can lead to inadequate cell migration and immunomodulation, which may, in turn, decelerate the healing process.[5] In another study, potential of a curcumin and phytic acid loaded polyvinyl alcohol hydrogel, reinforced with wood fiber for periosteal tissue engineering, was investigated. It was stated that combined use of curcumin and phytic acid led to immunomodulation by increasing IL10 and decreasing IL1B.[8] In a recent study, bilayer poly(ε-caprolactone)/gelatin fibers loaded with deferoxamine on the outer layer and aspirin and silicon nanoparticles

[a] Department of Biotechnology, Middle East Technical University, Ankara, 06800, Turkey. E-mail: tezcaner@metu.edu.tr
[b] Boron Research Institute, Turkish Energy Nuclear and Mineral Research Agency, Ankara, 06520, Turkey
[c] Department of Plastic and Reconstructive Surgery, Dr Rıdvan Ege Hospital, Ufuk University, Ankara, 06510, Turkey
[d] Department of Engineering Sciences, Middle East Technical University, Ankara, 06800, Turkey
[e] Center of Excellence in Biomaterials and Tissue Engineering, Middle East Technical University, Ankara, 06800, Turkey

on the inner layer were examined. It was reported that hierarchical fabrication ensured resemblance of the native periosteum, whereas aspirin, deferoxamine and silicon nanoparticles facilitated immunomodulation, angiogenesis and osteogenesis, in a rat subcutaneous implantation study.[9] Despite current developments, the need for a periosteum-mimetic implant capable of simultaneously supporting osteogenesis and modulating inflammatory responses remains clinically unmet.

Various natural and synthetic membranes have been investigated for guided bone regeneration to address this need. Fibroin (F) is a biocompatible and biodegradable protein-type biomaterial. F can be utilized in sponge, fiber, hydrogel and membrane forms, which makes it a versatile component for tissue engineering applications.[10] Biocompatibility and practicality of F also enabled its use in periosteal tissue engineering approaches. A recent study evaluated the use of F sponge covered with F mat, seeded with bone marrow mesenchymal stem cells (BMSCs) and endothelial progenitor cells, as an artificial periosteum. Alkaline phosphatase (ALP) activity assay and alizarin staining revealed that use of the developed artificial periosteum with osteogenic differentiation medium significantly increased osteogenic differentiation, compared to undifferentiated BMSCs seeded on tissue culture polystyrene (TCPS). However, differentiated BMSCs were not taken into comparison. It was also mentioned that compared to electrospun F and cell free scaffold groups, the cell seeded scaffold group significantly increased the bone volume to tissue volume ratio, in a rabbit critical size bone defect model.[11] Different from the aforementioned study using cell transplantation, the present work aims to promote healing through exosomes, which are less likely to cause tumor formation.[12] F-based scaffolds were often enriched with other biomaterials or bioactive molecules to improve bioactivity and resemblance to the native tissue.[13] In a recent study, electrospun F loaded with melatonin was reported to show similar characteristics in terms of the degradation rate, tensile strength and surface wettability. It was also mentioned that melatonin loading significantly increased osteogenic differentiation of rat BMSCs and tube formation of human umbilical vein endothelial cells (HUVECs), compared to the F group.[14] Sulfated alginate (sA) is a modified polysaccharide obtained by chemical modification of alginate. sA is reported to be an analogue of heparin.[15] Heparin binds proinflammatory cytokines and chemokines, inhibiting their interaction with corresponding cell surface receptors.[16] This resemblance makes sA a potent component of tissue engineering scaffolds, providing immunomodulation.[15] In a study, encapsulation of mesenchymal stem cell spheroids in the sA hydrogel was reported to lower deposition of fibrotic collagen, leading to accelerated healing of a rat muscle crush injury, compared to alginate.[17] Another study reported that sA supplemented cell culture medium led to significant decrease in expression of *TNFA* in THP-1 macrophages and IL6 in human chondrocytes.[18] In this study, the sA composite was incorporated into the F-based membrane structure to improve inflammatory response through cell–material interactions.

Exosomes are a subgroup of extracellular vesicles with the size between 30 and 200 nm, taking part in various processes such as tissue healing, immune reaction, cancer and cell communication.[19] Exosomes can be chemically modified, genetically engineered to contain a specific cargo, or loaded with drugs and nucleic acids. Signaling capacity, biocompatibility and modularity of exosomes enable exosomes to be used in tissue engineering applications.[20] In a study, aptamer and polyethyleneimine functionalized Schwann cell exosomes were immobilized on electrospun polycaprolactone fiber mats, to obtain an artificial periosteum. Fabricated implants were shown to increase osteogenesis, angiogenesis and neural regeneration in comparison to non-exosome containing groups, in a rat critical size bone defect model.[21] Exosomes from treated/induced cells were also used in a periosteal tissue engineering approach to improve biological response from recipient cells. In a study, the effect of exosomes in a tumor xenograft model with a critical-sized bone defect was investigated. Bone density scan revealed that the group with exosomes obtained from BMP-2 treated cells significantly increased bone volume, compared to the group containing untreated exosomes.[22] Both studies demonstrated improvement of periosteal regeneration due to exosomes, yet exact contents of the exosomes were not studied. Another recent work has demonstrated that decellularized porcine pericardial matrix bilayer patches loaded with adipose-derived stem cell exosomes can enhance wound healing by promoting re-epithelialization and angiogenesis through sustained release.[23] Collectively, these findings further underscore the considerable therapeutic potential of exosomes as versatile, cell-free mediators in tissue engineering.

Hydroxyapatite (HA) is a type of calcium phosphate present as the inorganic part of the bone extracellular matrix. HA was commonly doped with different elements to improve the biological properties of the material.[24] Osteogenic properties of HA and doped HA attract attention in periosteal tissue engineering strategies as well. In a study, the effect of HA scaffolds and cultivation conditions on the osteogenic and angiogenic potential of BMSC derived exosomes was investigated. 3D printed HA scaffolds were seeded with BMSCs and cultured under normoxic and hypoxic conditions. Obtained exosomes were used to treat HUVECs *in vitro* and the rat calvarial defect model *in vivo*. It was stated that compared to normoxic exosomes, hypoxic exosomes significantly increased viability and VEGF expression of HUVECs. It was also noted that expression of ALP and COL1 in hypoxic exosome treated tissue was significantly higher than that in normoxic exosomes.[25] Although the study revealed the potential of HA treated exosomes, untreated exosomes were not taken into consideration to assess the effect of HA treatment.

In our previous study, we have shown that HA doped with 8 mol% B and 4 mol% Zn provided optimal viability and osteogenic activity of human adipose derived mesenchymal stem cells (hADSCs) and the angiogenic effect in HUVECs.[26] The aim of this study was to develop osteogenic, angiogenic, and immunomodulatory membranes for periosteal tissue engineering applications. For this purpose, prior to exosome isolation, hADSCs were treated with cultivation media containing HA, B-doped HA or B and Zn dual-doped HA. Considering the current

knowledge of effects of exosomes from HA-treated cells, it was hypothesized that B and Zn-doping may further modulate osteogenic and inflammatory signaling pathways. Accordingly, exosomal content was characterized to enlighten changes in composition, due to different treatment conditions. Exosome enriched novel F/sA membrane groups were fabricated and characterized to obtain optimal biological response from recipient hADSCs, HUVECs and differentiated THP-1 macrophages. The study demonstrates that exosomes derived from cells treated with different HA types had varying responses involved in periosteal regeneration.

2. Materials and methods

2.1. Materials

Bombyx mori cocoons were purchased from Bursa Kozabirlik (Türkiye). Alginate, $(NH_4)_2HPO_4$, H_3BO_3, $Ca(NO_3)_2{\cdot}4H_2O$, $Zn(NO_3)_2{\cdot}6H_2O$, Na_2CO_3, LiBr, HSO_3Cl, CH_3NO, NaOH, acetone, NaCl, KCl, Na_2HPO_4, KH_2PO_4, ascorbic acid, dexamethasone, β-glycerophosphate, uranyl acetate, and Triton X-100 were from Sigma-Aldrich (USA). DMEM/F12, fetal bovine serum (FBS), trypsin/EDTA, penicillin/streptomycin, and RPMI 1640 were from Capricorn Scientific (Germany). Vascular cell basal medium (PCS-100-030) and the vascular endothelial cell growth kit (PCS-100-041) were from ATCC (USA), whereas phorbol 12-myristate 13-acetate (PMA), lipopolysaccharide (LPS), ATP and normocin were from InvivoGen (USA). ELISA kits were purchased from Cusabio (China) and RNA isolation, cDNA synthesis and PCR kits were from Roche (Switzerland). The bicinchoninic acid assay (BCA) kit and exosomal RNA isolation kit were from BioVision (Switzerland), whereas PicoGreen and alamarBlue™ dyes were supplied by Thermo Fisher Scientific (USA). Flow cytometry antibodies CD45 (304026), CD73 (344016), CD90 (555595) and CD105 (323203) were from Biolegend (USA).

2.2. Methods

2.2.1. Synthesis of HA groups. HA groups were synthesized by a microwave assisted wet precipitation method and characterized as described previously. HA, 8 mol% B containing 8B HA and 8 mol% B and 4 mol% Zn containing 8B 4Zn HA groups were chosen since they had maximum amounts of dopants that can be tolerated by hADSCs.[26] Briefly, $(NH_4)_2HPO_4$ and H_3BO_3 solutions were added to $Ca(NO_3)_2{\cdot}4H_2O$ and $Zn(NO_3)_2{\cdot}6H_2O$ solutions. The pH was set to 10.0 with NH_4^+ and the mixture was stirred at 600 rpm for 30 minutes. Then, the mixture was aged in a microwave oven at 600 W for 15 minutes. Finally, the precipitate was filtered and sintered at 500 °C for 2 h. Molar compositions of the HA groups are given in Table 1.

2.2.2. Fabrication and characterization of F/sA membranes

2.2.2.1. Isolation of F. F isolation began with the removal of sericin, which is the other component of the silk cocoon. For this purpose, 4.24 g of Na_2CO_3 was added to 1 L of boiling dH_2O. 5 g of silk cocoon pieces were boiled in this solution for 30 minutes to remove sericin. Then, fibroin was washed with dH_2O and dried at 50 °C. The dried fibroin was dissolved in 9.3 M LiBr in a 4 times volume of its dry weight. In order for the fibroin to dissolve completely, the mixture was incubated at 60 °C for 4 h. The resulting fibroin solution was dialyzed against distilled water for 2 days, by changing water 4 times a day. After dialysis, the fibroin solution was centrifuged at 20 000*g* for 15 min to remove the pellet and solid impurities. Concentration of the solution was determined gravimetrically, by drying 1 ml of the solution.[27] Concentration of the obtained fibroin solution was set to 8% with dH_2O and the solution was stored at 4 °C.

Table 1 Theoretical molar ratios of Ca, Zn, P and B in HA groups

	Ca (%)	Zn (%)	P (%)	B (%)
HA	61.54	0	38.46	0
8B HA	61.54	0	30.46	8
8B 4Zn HA	57.54	4	30.46	8

2.2.2.2. Sulfation and characterization of alginate. Alginate was sulfated by a single-step reaction. For this purpose, 50 g of alginate was dispersed in 1 L of 3.5% (v/v) HSO_3Cl solution in CH_3NO. Sulfation reaction was carried out at 60 °C for 4 hours. Then, sA was precipitated with acetone, dissolved in dH_2O and neutralized with 5 M NaOH. sA solution was dialyzed against dH_2O for 2 days, by changing water 4 times a day. Finally, dialyzed sA was lyophilized at −80 °C and stored at 4 °C, until use.[28] The presence of functional groups in the structure of sA was assessed using FTIR (Bruker IFS66/S, USA) in the 4000–400 cm^{-1} mid-infrared range. Sulfur content of the sA was determined by elemental analysis using a sulfur/carbon determinator (LECO, Denmark). The degree of sulfation (DS) was calculated according to eqn (1), where m_{sulfur} is the measured sulfur mass, MW_{sulfur} is the molecular weight of sulfur, $m_{monomer}$ represents the theoretical mass of alginate repeat units and $MW_{monomer}$ corresponds to the molecular weight of the alginate monomer unit.

$$DS\ (\%) = 100 \times \left(1 - \frac{m_{sulfur}/MW_{sulfur}}{m_{monomer}/MW_{monomer}}\right) \quad (1)$$

2.2.2.3. Fabrication of F/sA membranes. F/sA scaffolds were prepared by mixing 8% (w/v) F and 8% (w/v) sA solutions. In order to obtain different F/sA w/v ratios, prepared solutions were mixed at different volumes at a final volume of 5 mL [Table 2]. After mixing, solutions were poured in Teflon molds with a diameter of 4 cm and dried at room temperature.

2.2.2.4. Characterization of F/sA membranes

2.2.2.4.1. Morphological analysis. Morphology of F/sA scaffolds was visualized by using SEM (FEI NanoSEM, USA). Prior to

Table 2 F and sA weight ratios of F/sA scaffolds and volumetric ratios of used F and sA solutions

Group	F/sA (w/w)	8% F (mL)	8% sA (mL)
100 : 0	100 : 0	5.00	0
95 : 5	95 : 5	4.75	0.25
90 : 10	90 : 10	4.50	0.50
80 : 20	80 : 20	4.00	1.00

imaging, samples were sputter-coated with gold with a thickness of 3 nm.[29]

2.2.2.4.2. Water contact angle measurement. The water contact angle of scaffolds was measured, in order to determine the effect of the F/sA ratio on surface wettability. The water contact angle was determined using a goniometer (Attension, Biolin Scientific, Sweden) at 25 °C. dH_2O was chosen as the testing liquid and droplets were set to 7 μL. Contact angles were calculated using the Young–Laplace formula.[30]

2.2.2.4.3. Equilibrium swelling analysis. Water uptake percent of F/sA membranes was measured using a general gravimetric method. The dry weights of the 1 cm^2 samples were recorded, and then the samples were incubated at 37 °C in 10 mL of phosphate buffered solution (PBS, pH 7.4). After the 1st, 2nd, 4th, 8th and 24th hours of incubation, the surface of the samples was gently wiped with filter paper, and weights of the wet samples were measured. Finally, the water uptake percentages of the samples were calculated.[31]

2.2.2.4.4. Weight loss analysis. Initial weights of 1 cm^2 specimens were weighed and the samples were incubated in 10 ml of PBS, pH 7.4. At the end of the 1st, 4th, 7th, 10th and14th days, the samples were dried by lightly wiping with filter paper and lyophilization at −80 °C. After measuring the weights of the dried samples, the weight loss percentages were calculated.[32] Additionally, morphology of samples after 14 days of degradation was assessed by scanning electron microscopy (SEM) imaging.

2.2.2.4.5. Release study. F and sA release from weight loss analysis samples was determined using BCA and DMMB assays, respectively. BCA assay was performed according to the manufacturer's protocol, whereas DMMB assay was performed manually. Bovine serum albumin (BSA, 25 μg mL^{-1}–2 mg mL^{-1}) and sA (15.63 μg mL^{-1}–32 mg mL^{-1}) solutions in PBS were used as standards. DMMB solution was prepared by dissolving 1.15 mL of acetic acid, 608 mg of glycine, 320 mg of NaCl and 3.2 mg of DMMB in 200 mL of distilled water. The solution was filtered after setting the pH of the solution to 3.0. 200 μL of DMBB solution was mixed with 20 μL of the sample or standard. After a few seconds of shaking, the absorbance of the samples at 520 nm was recorded.[33]

2.2.2.4.6. Tensile test. The tensile test was performed on membranes with 4 cm length and 1 cm width, wetted in PBS (Univert, CellScale, Canada). Ultimate tensile strength, elastic modulus and strain percentage of periosteal implants were determined by applying a static tensile speed of 1 mm min^{-1}.[34]

2.2.3. *In vitro* studies

2.2.3.1. Cultivation of cells. hADSCs were isolated and characterized as reported elsewhere.[35] Required ethical approval for non-invasive clinical research was obtained from the TOBB University of Economics and Technology (KAEK-118/132). Stemness of the third passage of hADSCs was verified by using flow cytometry.[36] Percentage of the negative marker $CD45^+$ cells was 0.09%, whereas percentages of the positive markers $CD73^+$, $CD90^+$ and $CD105^+$ cells were 99.96, 98.51 and 97.93%, respectively (Fig. S1). Isolated hADSCs were cultivated in high glucose DMEM/F12 supplemented with 10% FBS and 10 U mL^{-1} Pen per Strep, in an incubator (5215, (MCO-5M-PE CO_2 Incubator, Panasonic, Japan) at 37 °C with 5% CO_2 and 95% humidity. The mentioned cultivation media were referred as F12. Cells were passaged when they reached 80% confluency, using 0.05% Trypsin/EDTA. Third passage cells were cryopreserved in 10% DMSO in FBS (v/v). Osteogenic medium was prepared by supplementing F12 with 50 μg mL^{-1} ascorbic acid, 10 mM β-glycerophosphate and 10^{-8} M dexamethasone. In studies with exosomes, media were supplemented with exosome depleted FBS. Human umbilical vein endothelial cells (HUVECs) were cultivated with vascular cell basal medium, supplemented with a vascular endothelial cell growth kit. Cells were passaged when they reached 80% confluency, using 0.05% Trypsin/EDTA. In studies with exosomes, media were supplemented with exosome depleted FBS. THP-1 monocytes were cultivated with RPMI 1640 medium supplemented with 10% FBS 10 U mL^{-1} Pen/Strep and 50 mg mL^{-1} normocin. Cells were passaged when they reached 2×10^6 cells per mL. In studies with exosomes, media were supplemented with exosome depleted FBS and no antibiotics were used during immunomodulation studies.

2.2.3.2. Isolation and characterization of exosomes

2.2.3.2.1. Exosome isolation. Exosomes from hADSCs treated with 0.5 mg mL^{-1} HA groups were isolated by ultracentrifugation.[37] For this purpose, 2×10^7 third passage cells were seeded into 175 cm^2 cell culture flasks and incubated for 24 hours. Then, the cells were washed with PBS and cell culture media were replaced with media containing exosome depleted FBS or exosome depleted FBS and HA groups. HA groups were chosen as HA, 8B HA and 8B 4Zn HA. Exosomes of untreated cells were referred to as the F12 group. After 48 hours of cultivation, the media were centrifuged at 480*g* for 5 minutes, at 2000*g* for 10 minutes and at 10 000*g* for 30 minutes. After each step, the pellet was removed and the supernatant was collected. Final centrifugation was performed at 100 000*g* for 70 minutes using an ultracentrifuge (Hitachi CP100WX, Japan). The pellet containing exosomes were resuspended in sterile PBS and stored at −80 °C, until use.

2.2.3.2.2. Characterization of exosomes. Transmission electron microscopy (TEM). Morphology of the isolated exosomes was investigated using transmission electron microscopy (TEM, FEI Tecnai G2 Spirit BioTwin, USA). First, 2 μL of the exosome suspension was loaded on a grid. Then, the grid was immersed in a drop of 2% uranyl acetate for negative staining. The stained grid was then washed with dH_2O twice and let dry.[38]

Nanoparticle tracking analysis. Concentration of exosomes isolated from cells treated with different HA groups was determined using nanoparticle tracking analysis (Nanosight NS300, Malvern, UK). For this purpose, 10 μL of exosomes were diluted to 1 mL. The particle size and concentration of the exosomes were recorded for each group.

Protein quantification. Exosomal protein amounts were quantified with a BCA assay kit and normalized to the particle number.[39] Samples were prepared by adding 20 μL of distilled water, 20 μL of 0.1% (w/v) Triton X-100 and 50 μL of BCA working solution into 20 μL of exosomes. After 1 hour of incubation at 37 °C, the absorbance at 562 nm was recorded. The amount of the protein was determined using the calibration curve constructed with BSA.

DNA quantification. Exosomal DNA content was quantified with the PicoGreen dye and normalized to the particle number.[39] For this purpose, 10 μL of distilled water and 50 μL of 0.1% Triton X-100 were added to 40 μL of exosomes. After lysis, 100 μL of PicoGreen solution was added and fluorescence with 480 nm excitation and 520 nm emission was recorded. The amount of the DNA was determined using the calibration curve constructed with bovine DNA (25 ng–1 μg).

RNA quantification. Exosomal RNA was isolated by using an exosomal RNA isolation kit (Biovision, Switzerland). 2 μL of isolated RNA samples were quantified by using a Take3 microvolume plate (Agilent, USA). Concentration of RNA was normalized with particle concentration.[39]

2.2.3.3. Sample preparation. HA groups were weighed and placed in falcon tubes, prior to sterilization. F/sA membranes were cut in 9 mm circles for ELISA studies and 35 mm circles for PCR studies. All samples were sterilized with 25 kGy γ-irradiation and stored at 4 °C, until use. Exosomes were loaded on sterile F/sA membranes by impregnation for 4 hours with a density of 10^7 particles per cm^2. Compositions of membrane groups loaded with exosomes are given in Table 3. For exosome studies membranes loaded with exosomes from untreated cells were denoted as F12. Membrane groups loaded with exosomes from HA, 8B HA or 8B 4Zn HA treated cells were labelled with the same name as the HA group used for treatment.

2.2.3.4. Cell viability and proliferation. Viability and proliferation of hADSCs seeded on samples were determined using alamarBlue assay.[40] First, sterile samples were placed in 48 well plates and the cells were seeded with a density of 5×10^3 cells per well. The percent reduction of alamarBlue™ dye was calculated as an indicator of cell viability and proliferation, on days 1, 4, 7, 10 and 14 of cultivation. Briefly, 10% (v/v) alamarBlue solution was prepared in phenol-free cell medium. The prepared solution was added to the wells and incubated for 4 hours. Then, alamarBlue solution was transferred to a new well plate and new cell culture media were added to the samples so that the cultivation continued. Absorbance of the alamarBlue solution was measured at 570 and 600 nm and percent reduction of alamarBlue™ was calculated according to the manufacturer's instructions.

Table 3 Composition of membrane groups loaded with exosomes

Group	F/sA membrane	Exosome loading	Exosome conditioning
95 : 5	95 : 5	No	Not applicable
F12	95 : 5	Yes	No
HA	95 : 5	Yes	HA
8B HA	95 : 5	Yes	8B HA
8B 4Zn HA	95 : 5	Yes	8B 4Zn HA

2.2.3.5. Osteogenic differentiation. Osteogenic differentiation analysis was performed on hADSCs to determine the effect of experimental groups on osteogenic differentiation. Cells seeded on TCPS and cultivated with F12 were used as a negative control ($TCPS^-$), while cells seeded on TCPS and cultivated with osteogenic cell medium were used as a positive control ($TCPS^+$). All groups except the TCPS – group were cultivated with osteogenic cell medium throughout the cultivation period. PCR analysis was performed to examine the osteogenic effect of the periosteal membranes with and without exosomes at the transcriptome level. Sterile samples were placed in 6-well cell culture dishes and cell seeding was carried out at 2×10^5 cells per sample. Following cultivation in osteogenic media for 14 days, total RNA was isolated. Following RNA isolation, cDNA was synthesized and PCR reaction analysis was performed (LightCycler® 48, Switzerland). Expressions of *COL1A1* and *RUNX2* were determined in proportion to *ACTB* expression.[41] Primer sequences are given in Table 4. In order to examine the effect of the groups on osteogenic differentiation at the proteome level, the amount of osteocalcin in the samples was determined by ELISA. The samples were placed in 48-well plates and cell cultivation was carried out using 2×10^4 cells per well. Following cultivation with osteogenic media for 14 days, the cells were lysed with distilled water and then frozen and thawed at −80 °C. The amount of OCN in the samples was determined using an ELISA kit. The results obtained were normalized according to the amount of DNA. For this purpose, the absorbance formed by interacting 50 μL of cell lysate with 50 μL of PicoGreen solution was measured with a spectrophotometer at 480 nm.[42]

2.2.3.6. Immunomodulation. Immunomodulatory properties of F/sA membranes loaded with F12, HA, 8B HA and 8B 4Zn HA

Table 4 Forward (F) and reverse (R) primer sequences used in qPCR studies

Gene	Primer	sequence (5′ → 3′)
ACTB	F	CACCATTGGCAATGAGCGGTTC
	R	AGGTCTTTGCGGATGTCCACGT
COL1A	F	GATTCCCTGGACCTAAAGGTGC
	R	AGCCTCTCCATCTTTGCCAGCA
RUNX2	F	CCCAGTATGAGAGTAGGTGTCC
	R	GGGTAAGACTGGTCATAGGACC
RPL13	F	CGCTCCAAACTCATCCTCTTC
	R	CTCTTCCTCAGTGATGACTCGAG
CASP1	F	GCTGAGGTTGACATCACAGGCA
	R	TGTCTGTCAGAGGTCTTGTGCTC
IL1B	F	CCACAGACCTTCCAGGAGAATG
	R	GTGCAGTTCAGTGATCGTACAGG
NFKB	F	GCAGCACTACTTCTTGACCACC
	R	TCTGCTCCTGAGCATTGACGTC
IL10	F	CATCAAGGCGCATGTGAACTC
	R	AATCGATGACAGCGCCGTAG
NOS3	F	ACCAGCACATTTGGGAATGG
	R	TCTGAGCAGGAGATGCTGTTG
VEGFA	F	TCACCATGCAGATTATGCGGA
	R	CACGCTCCAGGACTTATACCG

exosomes were investigated by using THP-1 monocytes as aforesaid. For this purpose, first, monocytes were differentiated into macrophages by incubation with 50 ng mL^{-1} PMA for 48 hours. Differentiated macrophages were removed from the cell culture dish by trypsinization and seeded on membranes or TCPS with a density of 1×10^6 cells per well in 6-well plates for PCR and 1×10^5 cells per well in 48-well plates for ELISA.[43] After 24 hours of attachment and resting, the cells were treated with 100 μg mL^{-1} LPS and incubated for 24 hours for activation of the TLR4 pathway.[44] The NLRP3 pathway was activated by priming with 100 μg mL^{-1} LPS for 4 hours and activation with 5 mM ATP for an additional hour.[45] The cells seeded on TCPS and treated with only PMA were used as a negative control, whereas the cells seeded on TCPS and treated with PMA and LPS or ATP were referred to as positive controls. Expression of *CASP1* and *IL1B* was determined by qRT-PCR and concentration of CASP1 was assessed by ELISA (Cusabio, China) in ATP treated cells.[43] Expressions of *NFKB* and *IL10* were determined by qPCR and concentration of secreted IL1B was assessed by ELISA (Cusabio, China) in LPS treated cells. The fold change in expressions was calculated by using *RPL13* as the housekeeping gene, whereas amounts of CASP1 and IL1B were normalized to DNA, which was quantified using the PicoGreen dye.[46] Primer sequences are given in Table 4.

2.2.3.7. Angiogenesis. The effect of F/sA membranes loaded with F12, HA, 8B HA and 8B 4Zn HA exosomes on angiogenesis was investigated by using HUVECs. The cells seeded on TCPS were used as the control. Sterile samples were placed in 6-well cell culture dishes and cell seeding was performed at 1×10^6 cells per sample for qRT-PCR studies. Total RNA was isolated after 3 days of cultivation. Relative expressions of *NOS3* and *VEGFA* were determined by using *ACTB* as the housekeeping gene.[47] Primer sequences are given in Table 4. In order to examine the effect of the groups on angiogenesis at the proteome level, the amount of VEGFA in HUVECs seeded on the membranes was determined by ELISA. The membranes were placed in 48-well plates and cell seeding was carried out with a density of 1×10^5 cells per well. After 3 days of cultivation, the amount of VEGFA in the samples was determined with an ELISA kit, according to the manufacturer's protocol (Cusabio, China).

2.3. Statistical analysis

Significant differences between groups were assessed by using one-way analysis of variance (ANOVA), whereas multiple comparisons were performed using Tukey's comparison test (SPSS-26 Software, SPPS Inc., USA). A single asterisk (*) was used to refer to statistical significance, whereas double and triple asterisks denote significantly the highest and the lowest groups, respectively.

3. Results and discussion

3.1. Characterization of F/sA membranes

Alginate and sA were characterized using FTIR spectroscopy, in order to confirm sulfation (Fig. 1a). –OH (3224 cm^{-1}), –COO– (1408 and 1597 cm^{-1}) and COC (1026 cm^{-1}) peaks of alginate were observed for both samples.[48] Unlike the alginate spectrum, the sA spectrum had a peak around 1209 cm^{-1} corresponding to S=O symmetric stretching and another peak around 820 cm^{-1} representing S–O–C.[49,50] The DS was determined as 40.87 ± 0.16% (n = 3), which falls within the range reported for sA. Previous studies have shown that the sulfation degree is dependent on chlorosulfonic acid concentration and excessive sulfation may lead to polymer chain degradation. Therefore, the obtained sulfation level may reflect a balance between functional modification and preservation of polymer integrity.[51]

Morphology of F/sA scaffolds was investigated using SEM (Fig. 1b–e). Overall, all scaffolds were nonporous, with minor microcracks. However, it was noticed that the surface of the scaffolds became rougher with increasing sA content. It was reported that the fabrication method can affect the morphology of F membranes. In a similar study, air dried fibroin membranes, whose solvent was formic acid, were reported to have smooth morphology.[52] In another study, electropolymerized F membranes were noted to have a rougher surface with nanopores.[53] In addition to fabrication parameters, combination of different materials with F can also play a role in the morphology of membranes. It was reported that addition of 30% (v/v) polyvinyl alcohol to F resulted in a microporous structure, whereas the same ratio of glycerol yielded a rougher surface with no pores.[54] Current findings are consistent with reports that membrane morphology can vary depending on the fabrication method and composite composition, suggesting that incorporation of sA contributes to the observed surface roughening.

Water uptake analysis was performed by a gravimetric method (Fig. 1f). It was shown that all F/sA groups reached their maximum swelling in 1 hour. It was revealed that water uptake of 5% and 10% sA containing membranes was significantly higher than that of the 100% F containing 100 : 0 group. It was also noticed that starting from the 4th hour, the water uptake percentage of the 80 : 20 group was significantly lower than that of the 100 : 0 group.

F/sA membranes were subjected to weight loss analysis in order to investigate the *in vitro* stability of the samples (Fig. 1g). It was found that the sA percentage led to an increasing weight loss trend, with the 80 : 20 group having significantly the highest weight loss (31.67 ± 2.52% at day 14, n = 3) at all time points. It was also noticed that weight loss occurred mainly on day 1. This was expected since sA is a water-soluble polymer and is not crosslinked.[28] In water uptake analysis, it was observed that even though addition of 5% and 10% sA led to significant increase, 20% resulted in significant decrease, compared to the F membrane. Considering the water uptake and weight loss analyses together, it was concluded that lower water uptake of the 20% sA containing group was due to early weight loss. This may reflect a burst-like release behavior associated with higher sA content, which, while potentially beneficial for early signaling, may limit long-term structural performance. Weight loss analysis was also verified using SEM imaging (Fig. 1h–k). It was observed that after 14 days of

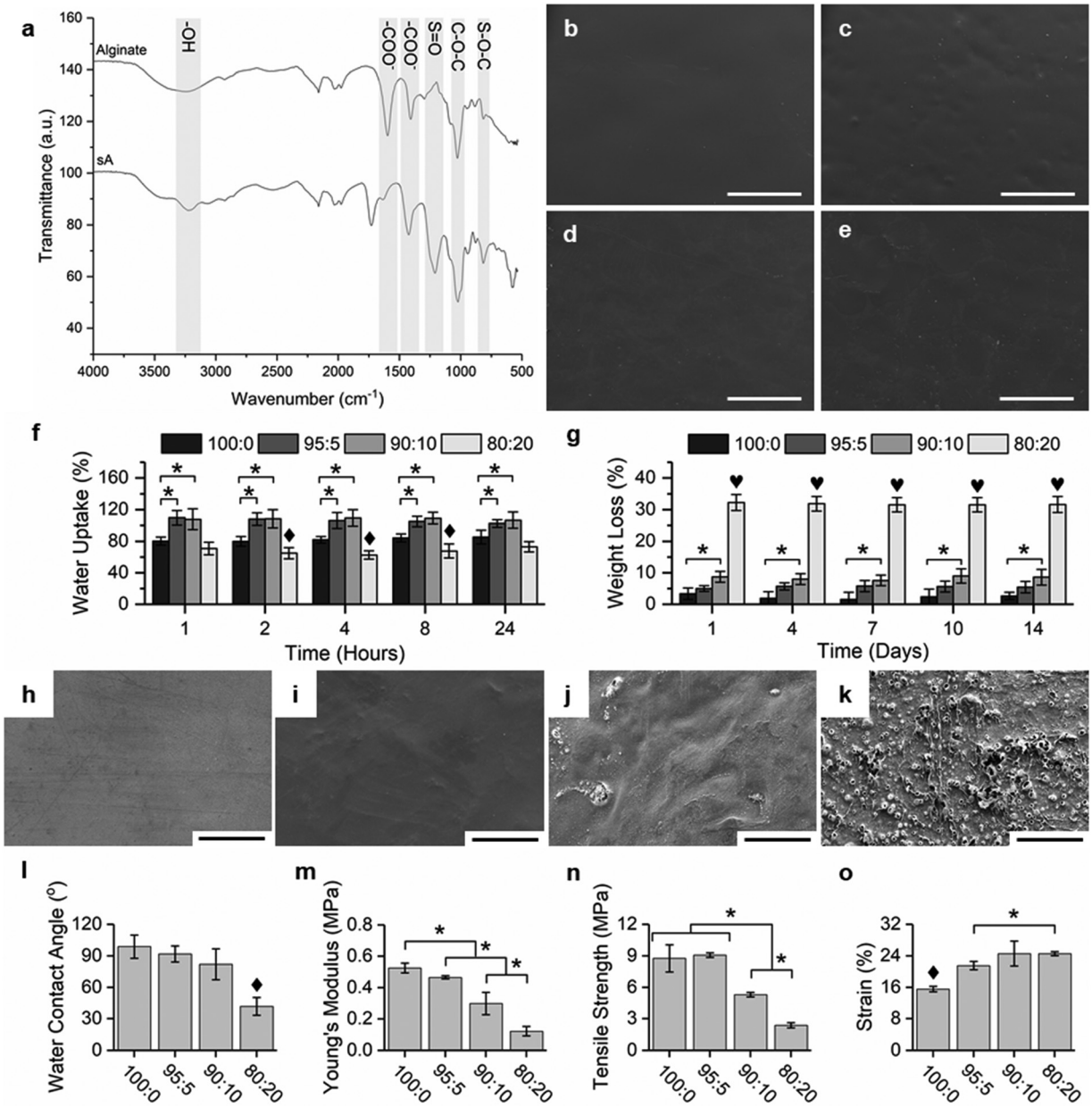

Fig. 1 FTIR spectra of alginate and SA (a). 100× SEM images of 100 : 0 (b), 95 : 5 (c), 90 : 0 (d) and 80 : 20 (e) F/sA membrane groups (scale bar: 1 mm). 24-hour water uptake (f) and 14-day weight loss (g) profiles of membrane groups ($n = 3$, $p < 0.05$). 1000× SEM images of 100 : 0 (h), 95 : 5 (i), 90 : 0 (j) and 80 : 20 (k) membrane groups after 14 days of weight loss analysis (scale bar: 100 μm). Water contact angle (l), Young's modulus (m), tensile strength (n) and (o) percent strain of membrane groups ($n = 3$, $p < 0.05$). A single asterisk (*) refers to a significant difference, whereas diamond (♦) and heart (♥) symbols denote the significantly lowest and highest groups, respectively.

incubation, 100 : 0, 95 : 5 and 90 : 10 groups presented their integrity, whereas visible deformations were present in the 80 : 20 group.

Surface wettability of the F/sA scaffolds was determined by water contact angle measurement (Fig. 1l). It was found that increasing sA content led to a decreasing water contact angle trend, with the 80 : 20 group having significantly the lowest water contact angle (41.79 ± 8.46°, $n = 3$). It is known that a scaffold's composition and morphology affect its surface wettability. In a study, lyophilized fibroin sponge coated with electrospun fibroin fibers was found to have a water contact angle of around 42°.[11] Another study reported that the fibroin membrane had a water contact angle of around 90°.[55] It was also stated that coating of polyether sulfonate fibers with sA lowers the water contact angle from around 75° to 38°.[56] It was also known that alginate is highly hydrophilic.[57,58] The reduction in water contact angle with increasing sA content aligns with previous reports on the hydrophilic nature of alginate and sulfated polymers, supporting the role of sA incorporation in enhancing surface wettability.

In order to determine the mechanical properties of the F/sA membranes, a tensile test was performed (Fig. 1m–o). Young's

modulus and tensile strength decreased due to increasing sA concentration, while the elongation percentage significantly increased. In a study examining the properties of membranes containing various amounts of F and alginate, it was found that alginate content up to 50% increased the percentage of elongation due to the increase in intramolecular hydrogen bonds.[59] In another study examining the effect of increasing F percentage on the mechanical properties of alginate membranes, it was stated that up to 60% F increased the mechanical tensile strength.[60] These trends are in agreement with previously reported effects of alginate incorporation on F-based membranes, suggesting that increased sA content contributes to enhanced flexibility at the expense of stiffness.

Release of F and sA during *in vitro* biodegradation was monitored using BCA and DMMB assays, respectively (Fig. 2a and b). In concordance with the weight loss, the highest release of F and sA was observed for the 80 : 20 group. sA release was found to be increasing with the increasing sA ratio of the groups. It was also noted that F release was similar for SA increase, indicating that release of sA triggered the release of F as well. SEM analysis after weight loss analysis also revealed visible degradation in the 80 : 20 group (Fig. 1k). This observation may be explained by increased exposure of polymer chains to the aqueous environment, consistent with reported relationships between scaffold structure and hydrolytic degradation.[61] sA was found to reduce inflammation through decreasing expression of TNF-α in macrophages.[18] Periosteum's healing process starts with inflammation taking up to 48 h.[62] Hence, the membrane groups were not crosslinked to allow sA to be released during the acute inflammation phase.

In vitro biocompatibility of F/sA membranes was investigated, in order to determine effect of sA concentration on cell viability and proliferation (Fig. 2c). On day 1, it was found that all groups had significantly higher cell viability than the TCPS control group. Starting from day 4, it was revealed that 100 : 0 and 95 : 5 groups showed significantly higher reduction of alamarBlue™ than that of the other groups. On days 10 and 14, viability of cells seeded in the 80 : 20 group was significantly the lowest. According to the cell viability and proliferation assay, 5% and 10% sA contents were considered as eligible for further studies. Final decision on F/sA membranes was made according to their immunomodulatory properties.

Immunomodulatory properties of the F/sA membranes were assessed by using THP-1 monocytes. First, monocytes were differentiated into macrophages with PMA.[63] Differentiated cells were then treated with LPS to activate the TLR4 pathway and stimulate the production of proinflammatory cytokines.[64] Alleviation of the TLR4 pathway is considered to be crucial for

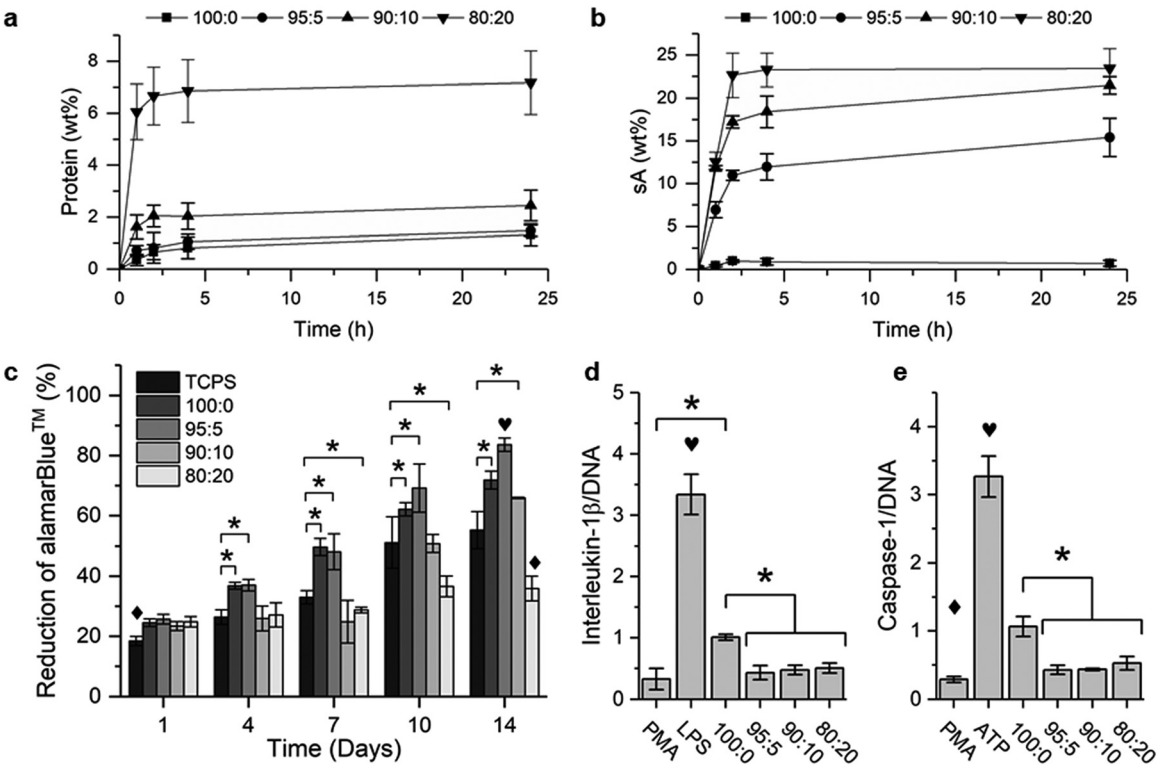

Fig. 2 Protein (a) and sA (b) release percentages from F/sA membrane groups (n = 3). (c) Percent reduction of alamarBlue™ by hADSCs seeded on F/sA membranes. Cells seeded on TCPS were used as a control group (n = 4, $p < 0.05$). (d) Extracellular IL1B from PMA differentiated and LPS induced THP-1 cells seeded on F/sA membranes. PMA differentiated cells seeded on TCPS were used as a negative control, whereas PMA differentiated and LPS induced cells seeded on TCPS were used as a positive control (n = 4, $p < 0.05$). (e) Intracellular CASP1 from PMA differentiated and ATP induced THP-1 cells seeded on F/sA membranes. PMA differentiated cells seeded on TCPS were used as a negative control, whereas PMA differentiated and ATP induced cells seeded on TCPS were used as a positive control (n = 4, $p < 0.05$). A single asterisk (*) refers to a significant difference, whereas diamond (♦) and heart (♥) symbols denote the significantly lowest and highest groups, respectively.

osseointegration, due to the crosstalk occurring between bone and immune cells.[65] Therefore, levels of Il-1β were investigated to examine the immunomodulatory effect (Fig. 2d). It was found that the cells seeded on TCPS and stimulated with LPS presented significantly higher Il-1β than the cells seeded on TCPS and differentiated with PMA only. Il-1β from cells seeded on all membrane groups and stimulated with LPS were significantly lower than that of the LPS group, for all groups. Notably Il-1β levels of PMA differentiated cells were similar to that of F/sA 95 : 5, 90 : 10 and 80 : 20 groups. For the other study, the cells were treated with ATP to induce formation of NLRP3 inflammasomes.[66] NLRP3 inflammasomes play a role in both inflammatory signaling and innate immune, which can cause rejection of the implant.[67] Hence, concentration of caspase-1 was investigated to examine the immunomodulatory properties of membrane groups (Fig. 2e). ELISA revealed that ATP treatment significantly increased caspase-1 levels in all groups. Similar to Il-1β, caspase-1 levels were significantly lower for all membrane groups, compared to the ATP group consisting of cells seeded in TCPS. Again, the sA ratio more than 5% did not lead to any significant decrease. It was previously reported that electrospun F fibers did not contribute to immunomodulation of RAW 264.7 macrophages.[29] However, it was also mentioned that immunomodulatory properties of F depend on the structure and processing of the scaffold.[68] Moreover, sA was found to act as an immunomodulatory biomaterial. It was reported that sA hydrogels decreased expression of TNF-α of mouse bone marrow derived macrophages primed with LPS and IFN-γ.[69] These findings indicate a balance between structural stability and bioactivity, where increasing sA content enhances biological response while accelerating degradation and compromising mechanical integrity. Considering that sA content more than 5% led to significantly lower cell viability and did not significantly decrease Il-1β and caspase-1 levels, it was concluded that the F/sA 95 : 5 group would be used for further studies.

3.2. Properties of exosome groups

The morphology of exosomes isolated from the F12 group was examined by TEM (Fig. 3a). Exosomes were observed as round shaped and intact vesicles.[38] The particle size of exosomes isolated from different experimental groups was determined by nanoparticle tracking analysis (Fig. 3b). The average sizes of all groups were similar (164–175 nm) and found to be in the range of 30–200 nm, which was accepted for exosomes.[19] The effect of treatment on exosome yield was also investigated (Fig. 3c). It was determined that the exosome concentration obtained from cells treated with 8B HA was significantly higher than that of the F12 group that was not subjected to any treatment. No differences were found between other groups. It was stated that 4×10^7 stem cells can produce 3–3.5 $\times$ 10^{10}

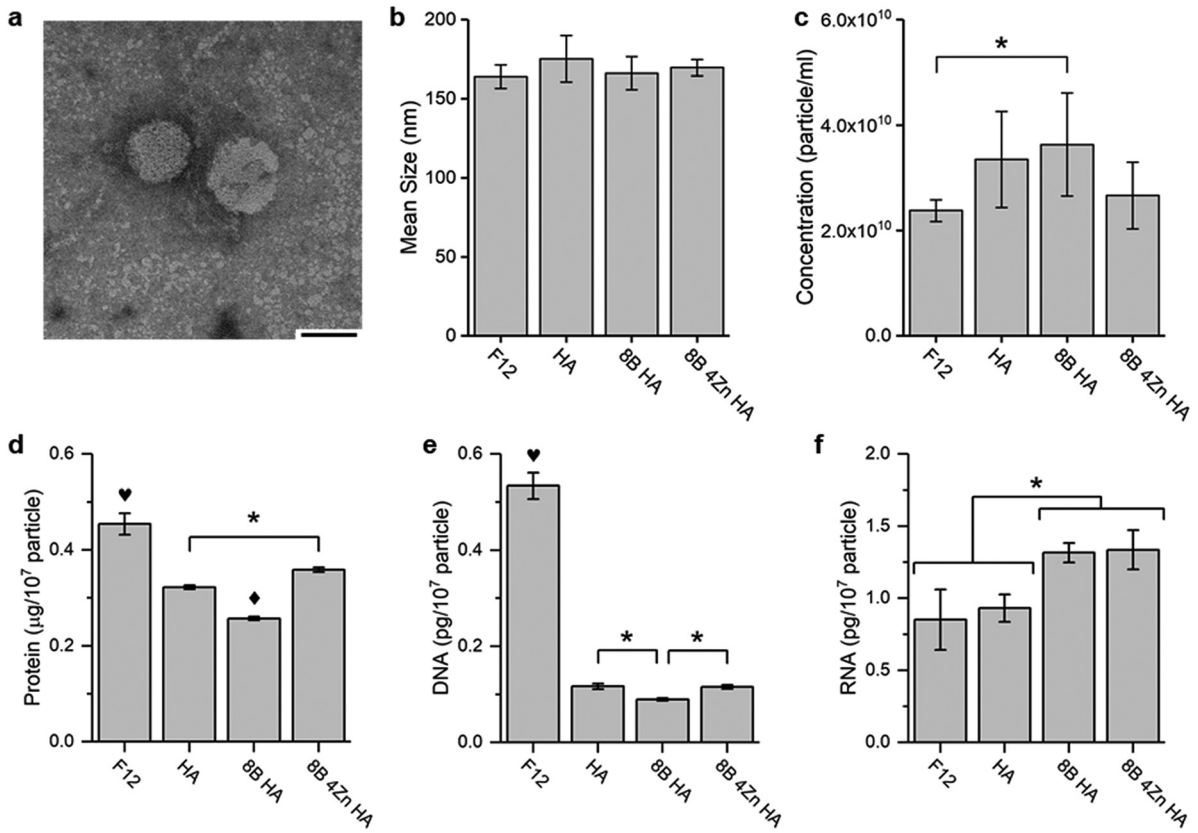

Fig. 3 (a) TEM image of exosomes of the F12 group (scale bar: 50 nm). Mean particle size (b) and concentration (c) of exosome groups (n = 3, $p < 0.05$). Protein (d), DNA (e) and RNA (f) contents of exosome groups per 10^7 particles (n = 3, $p < 0.05$). A single asterisk (*) refers to a significant difference, whereas diamond (♦) and heart (♥) symbols denote the significantly lowest and highest groups, respectively.

particle exosomes within 48 hours.[70] The observed exosome yield from HA-treated cells was within the range reported for stem cell-derived exosomes, suggesting that HA treatment did not negatively affect exosome secretion capacity. No significant difference was detected between the average sizes of the exosome groups. This may indicate that the isolation method rather than HA treatment influenced particle size distribution.[71] Minimal Information for Studies of Extracellular Vesicles (MISEV) guidelines states that comprehensive extracellular vesicle characterization ideally includes assessment of particle size, protein content and morphology as well as canonical surface and cytosolic markers and the particle-to-protein ratio.[72] In this study, classical exosomal protein markers and quantitative purity metrics were not evaluated, as the primary objective was comparative assessment of hydroxyapatite preconditioning effects rather than extensive extracellular vesicle subclass profiling. Future studies incorporating marker-based validation can enable more definitive identification and characterization of these exosome groups.

Protein content of exosome samples was determined by BCA (Fig. 3d). The amount of exosomal protein was normalized to the exosome concentration so that the exosomal content could be evaluated independent from concentration.[39] It was determined that the amount of exosomal protein of the 8B HA group was the lowest. In addition, it was determined that all HA groups caused a significant decrease in the amounts of exosomal protein. It has been reported in the literature that more than 40 000 proteins were detected in the exosomes of 10 species. It was also stated that these proteins may belong to general processes such as cargo and exosome release and membrane fusion and may also be associated with carcinoma, sarcoma, melanoma, neurological disorders, cardiovascular diseases, and immune response.[73] This reduction suggests that HA preconditioning may influence exosomal cargo composition rather than vesicle production. Exosomal DNA content was measured using the PicoGreen dye (Fig. 3e). It was determined that the amount of exosomal DNA significantly decreased in all groups treated with HA. Significantly, the lowest amount of DNA/exosome was detected in the 8B HA group. It has been stated in the literature that exosomal DNA is associated with various processes such as cell proliferation and programming of immune cells.[74] Hence the reduction in DNA content observed in HA-treated groups may indicate altered cargo packaging. In order to examine the effect of the amount of RNA in exosomes of the experimental groups, RNA amounts of the isolated samples were determined spectrophotometrically (Fig. 3f). When the effects of treatment of ADSCs with HA groups on their exosomal RNA contents were examined, it was determined that 8B HA and 8B 4ZnHA groups caused a significant increase in the amount of exosomal RNA compared to F12 and HA groups. In a study comparing the RNA contents of exosomes obtained from BMSCs and ADSCs, it was stated that adipose-derived stem cells contain RNAs belonging to osteogenic genes such as ALP.[75]

3.3. *In vitro* evaluation of exosome loaded F/sA membranes

The effect of exosomes on the viability and proliferation of hADSCs was determined by alamarBlue assay (Fig. 4a). On day 1, cell viability and proliferation in the HA, 8B HA, and 8B 4Zn HA groups were significantly higher compared to the 95 : 5 and F12-containing groups. At later time points (days 7 and 14), the percent reduction of alamarBlue™ in the 8B 4Zn HA group (67.83 ± 1.06 on day 14, $n = 4$) was significantly higher than that of the 95 : 5 group ($60.98 \pm 3.84\%$ on day 14, $n = 4$). This aligns with previous reports, indicating that exosomes can support cellular viability. In a study conducted using exosomes obtained from induced pluripotent cells, it was reported that the mentioned exosomes increased the viability of human dermal fibroblasts.[76] In another study, it was stated that exosomes isolated from hADSCs at a concentration of 2.14×10^{10} particles per mL did not cause a significant change in cell viability on the SKINETHIC™ skin model.[77] 14-Day morphology of cells was examined using SEM imaging (Fig. 4b–f). All groups were found to be covered with sheets, indicating viability and proliferation.[78] F was reported to enable formation of cell sheets.[79] This suggests that F contributed to structural cell organization, yielding a similar appearance between groups, despite the statistical significance of percent reduction of alamarBlue™ on day 14.

Osteogenic differentiation of hADSCs seeded on the membranes was studied to determine the effect of experimental groups on osteogenic differentiation. It was observed that the osteogenic cell medium caused a significant increase in *COL1A1* and *RUNX2* gene expressions and the amount of osteocalcin (Fig. 4g and h). Considering *COL1A1* and *RUNX2* gene expressions, it was determined that the 8B HA group had osteogenic activity similar to the TCPS$^+$ group and significantly higher than the 95 : 5 group. Unlike the gene expression analysis results, the amount of OCN was significantly higher in the HA (1.62 ± 0.06, $n = 4$) and 8B 4Zn HA (1.50 ± 0.12, $n = 4$) groups compared to the other groups (Fig. 4i). *COL1A1* gene expression is regulated by MRTF-A activation as a result of the RHOC/ROCK, TGF-β and WNT/CTNNB pathways.[80] RUNX2 gene expression is regulated by the Jagged/NICD, WNT/CTNNB, BMP/SMAD and TGFB/SMAD pathways, as well as directly by vitamin D.[81] Similarly, OCN is regulated by WNT/CTNNB and RUNX2, in addition to vitamins D and K. Additionally, OCN synthesis occurs later than *COL1A1* and *RUNX2* expression.[3] It is thought that the differences observed in gene expression analysis and ELISA results may be due to the activation of different pathways or the synthesis pathway of osteocalcin, a late osteogenic protein, activated sufficiently after 2 weeks of cultivation. These findings suggest that HA-conditioned exosomes may influence early osteogenic signaling pathways. Further studies (such as ALP activity assay) can further validate early osteogenic commitment observed at gene and protein levels.[82]

In order to examine the effects of exosome groups on *in vitro* inflammation in samples treated with LPS, the expression of *NFKB* and *IL10* was determined relative to *RPL13* expression [Fig. 5a and b]. Additionally, the amount of extracellular IL1B was determined by ELISA (Fig. 5c). The results obtained were normalized with the amount of DNA.[46,83] As a result of the analyses, it was determined that LPS treatment significantly increased *NFKB* gene expression and the amount of Il-1β, and

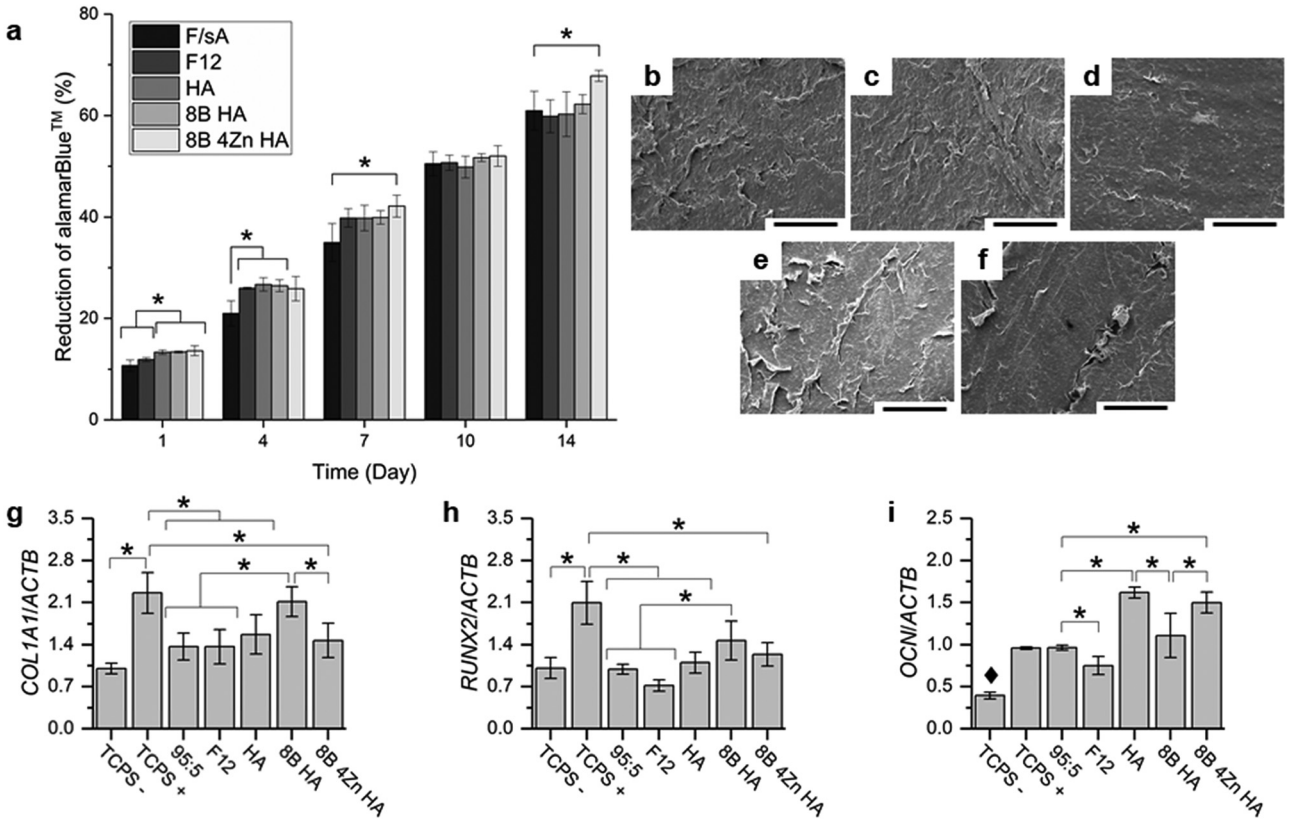

Fig. 4 (a) Percent reduction of hADSCs seeded on the membranes (n = 4, $p < 0.05$). 1000× SEM images of hADSCs cultivated on 95 : 5 (b), F12 (c), HA (d), 8B HA (e) and 8B 4Zn HA (f) groups for 14 days (scale bar: 100 μm). Expression of *COL1A1* (g) and *RUNX2* (h) relative to *ACTB* of the stem cells seeded on different membranes (n = 3, $p < 0.05$). (i) Relative OCN amount released from hADSCs seeded on the membranes, relative to DNA amounts (n = 4, $p < 0.05$). TCPS stands for cells cultivated on TCPS with cultivation media, while TCPS$^+$ refers to cells cultivated on TCPS with osteogenic media. A single asterisk (*) refers to a significant difference, whereas diamond (♦) denotes the significantly lowest group.

significantly decreased *IL10* gene expression. It has been determined that F/sA membranes have an immunomodulatory effect by significantly reducing the amount of IL1B (~2.48-fold) and increasing *IL10* gene expression (~1.87-fold). When exosome contributions were examined, it was determined that F12, HA, and 8B 4Zn HA groups showed a significant decrease in *NFKB* gene expression, which is an inflammation marker, and anti-inflammatory *IL10* gene expression, compared to the 95 : 5 group. *NFKB* gene expression can be activated by IL1B and is also regulated by TLRs, TCN and TNFR.[44,84] For this reason, it is thought that analyzing the expressions of other genes belonging to these pathways is necessary to explain the current situation. *IL10* gene expression was similar to IL1B. *IL10* expression of the 95 : 5 group was significantly higher than that of the 8B HA and 8B 4Zn HA groups. *IL10* expression in macrophage cells is regulated by activation of ERK protein following TLR2 and TLR4 activation.[85] Similarly, IL1B is regulated by TLR activation following LPS stimulation.[44]

In order to examine inflammasome formation in samples treated with ATP, the expression of *CASP1* and *IL1B* genes was determined in proportion to *RPL13* gene expression (Fig. 5d and e). In order to examine inflammasome formation at the proteome level, the amount of CASP1 in the cells was determined by ELISA (Fig. 5f). The results obtained were normalized according to the amount of DNA. As a result of stimulation of macrophages with ATP, NLRP3 inflammasomes were formed. As a result, CASP1 levels increase, which, in turn, increases IL1B levels. For this reason, it was aimed to investigate the expression levels of the mentioned genes.[43] As a result of the analyses, it was determined that exosome contributions did not have any effect on the *IL1B* expression of ATP-induced macrophages. Consistent with previous analysis, it was determined that the 95 : 5 group caused a significant decrease in *CASP1* expression and protein amount compared to the ATP group. Additionally, considering exosome contributions, F12, HA and 8B HA groups were found to show increased *CASP1* expression compared to the 95 : 5 group. Similar results could not be obtained for the amount of CASP1. It was determined that the amount of intracellular CASP1 in the 8B 4Zn HA group (0.90 ± 0.10, n = 4) was significantly higher than that of other exosome loaded groups (0.20 ± 0.05 for the HA group, n = 4). It has been reported that Zn may influence CASP1 activation.[86,87] Therefore, the elevated CASP1 levels observed in the 8B 4Zn HA group may suggest a potential association between zinc incorporation and inflammasome-related signaling. However, further mechanistic studies are required to clarify this relationship.

In order to examine the effect of the groups on angiogenesis by the expression of *NOS3* and *VEGFA* (Fig. 6a and b), and the

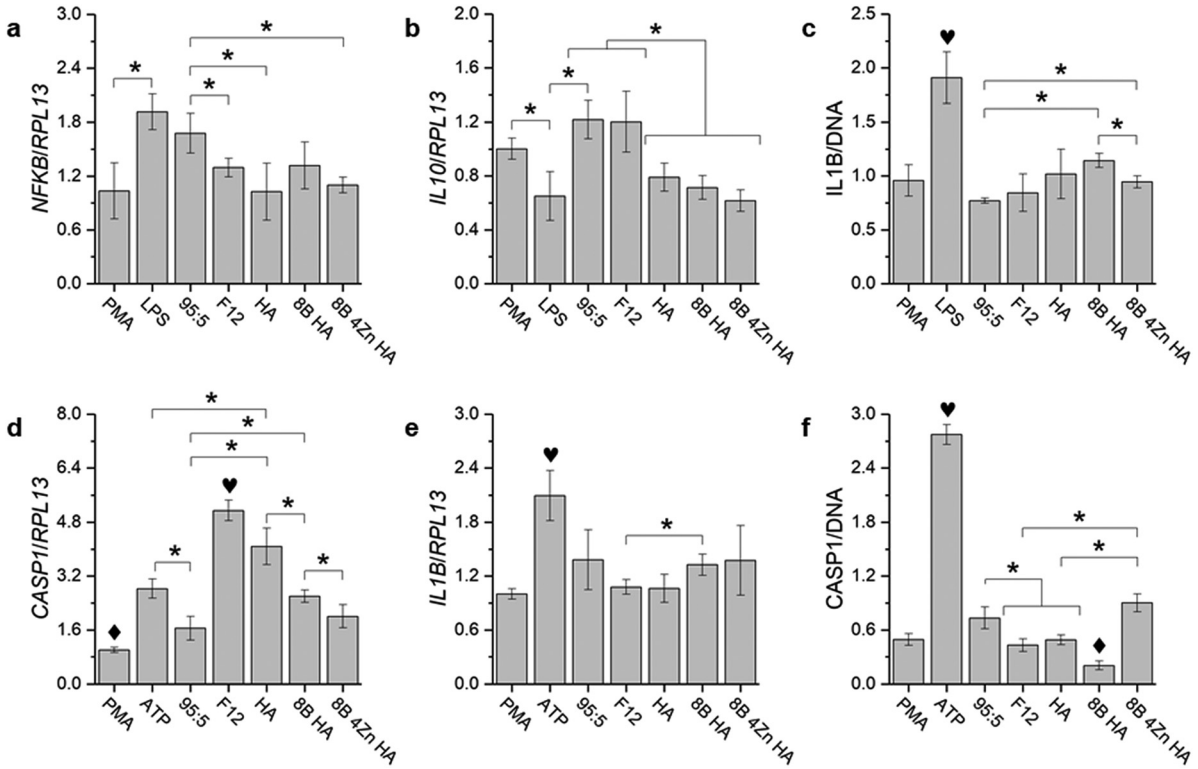

Fig. 5 Expression of *NFKB* (a) and *IL10* (b) relative to *RPL13* from PMA differentiated and LPS treated THP-1 macrophages seeded on groups ($n = 3$, $p < 0.05$). (c) Relative IL1B amount released from THP-1 macrophages, relative to DNA ($n = 4$, $p < 0.05$). *CASP1* (d) and *IL1B* (e) expression of PMA differentiated and ATP treated THP-1 macrophages seeded on groups relative to *RPL13* ($n = 3$, $p < 0.05$). (f) Relative amount of CASP1 released from THP-1 macrophages, relative to DNA ($n = 4$, $p < 0.05$). A single asterisk (*) refers to a significant difference, whereas diamond (♦) and heart (♥) symbols denote the significantly lowest and highest groups, respectively.

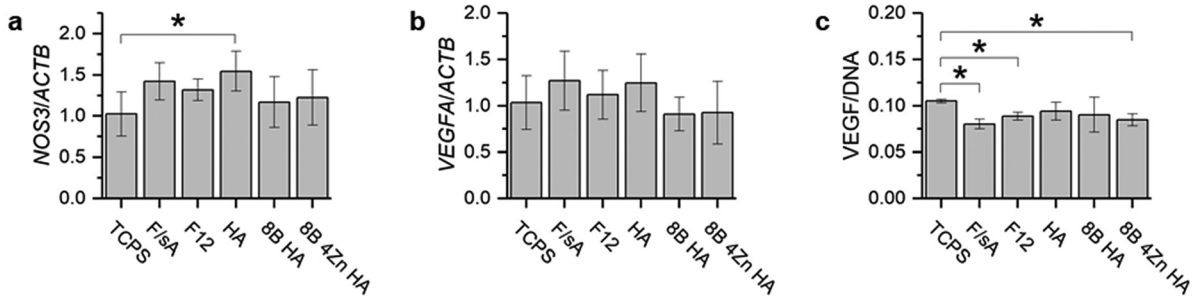

Fig. 6 Expression of *eNOS* (a) and *VEGFA* (b) and the relative amount of VEGFA (c) of HUVECs treated with membrane groups ($n = 4$, $p < 0.05$). A single asterisk (*) refers to statistical significance.

relative amount of VEGFA in HUVECs were determined (Fig. 6c). Although no difference in *VEGFA* expression was detected, it was determined that VEGFA amounts of the 95 : 5, F12 and 8B 4Zn HA groups were significantly lower than that of the TCPS group. It was also found that the expression of *NOS3* of the HA group (1.02 ± 0.27, $n = 3$) was significantly higher than that of the TCPS group (1.54 ± 0.24, $n = 3$). It was mentioned that exosomes may play an angiogenic or anti-angiogenic role. Angiogenic signals in the exosome cargo can be VEGF, MMP or miRNAs, while anti-angiogenic signals can be angiopoietin, angiostatin and collagen.[88] Stem cell exosomes can increase the expression of angiogenic genes with miRNAs, as well as anti-angiogenic signals with VEGF inhibition. Considering the available data, it has been determined that the HA group has the potential to support angiogenesis. Further studies incorporating functional assays such as tube formation can further clarify this angiogenic potential.[89]

4. Conclusion

In this study, for the first time, F/sA composite scaffolds loaded with exosomes of hADSCs, which were treated with pure and

doped HA, were developed for periosteal tissue engineering. It was revealed that increasing sA led to an increasing water uptake trend except for the 20% sA containing 80 : 20 group, which had significantly the highest degradation rate, which was also verified by SEM. The water contact angle, Young's modulus and tensile strength of the 80 : 20 membrane group were also significantly the lowest due to hydrophilic and non-crosslinked sA. Weight loss and release of F were accelerated by 20% sA, which was associated with availability of F chains for hydrolysis. An F/A ratio of 95 : 5 was found to increase 14-day cell viability and proliferation (∼16%) as well as decrease the CASP1 (∼60%) and IL1B (∼53%) levels, compared to the ratio of 100 : 0. Hence the 95 : 5 membrane group was used in further studies. Exosomes were isolated from hADSCs treated with different non-doped and doped HA groups to evaluate changes in protein, DNA and RNA levels, for the first time as well. Exosome yield was found to increase with B by ∼53%, relative to the untreated group. HA treatment led to decrease in protein and DNA in general. Interestingly, compared to the untreated group F12, RNA content was found to be significantly higher for B-doped HA (∼53% increase) and B and Zn doped HA (∼57% increase) groups, indicating that dopants also play a role in composition of exosomes. It was revealed that exosome loading in general significantly increased initial attachment and proliferation of hADSCs. Osteogenic differentiation was supported by HA, 8B HA and 8B 4Zn HA groups. Exosome loaded groups were also found to be immunomodulatory except for the 8B 4Zn HA group, which increased CASP1 (∼23% increase compared to the 95 : 5 group). Overall, it was shown that the exosome loaded F/sA membrane holds potential due to its regenerative and immunomodulatory properties. Treatment with HA and doped HA significantly alters exosomal contents and reactions of recipient cells. These findings provide preliminary insight into dopant-dependent modulation of exosomal composition and cellular responses, supporting their potential future application in tissue engineering strategies. Future studies incorporating comprehensive EV characterization, cargo profiling, and *in vivo* applications may further clarify the translational relevance of these findings.

Conflicts of interest

The authors declare no conflict of interest.

Data availability

Flow cytometry analysis of the isolated hADSCs has been provided as part of the Supplementary information.

Supplementary information (SI) is available. See DOI: https://doi.org/10.1039/d5tb02784e.

Acknowledgements

The authors would like to thank the Turkish Energy Nuclear Mineral Research Agency – Boron Research Institute (TENMAK BOREN) and Center of Excellence in Biomaterials and Tissue Engineering (BIOMATEN) for providing research infrastructure. The authors also acknowledge financial support from the Scientific and Technological Research Council of Turkey (TUBITAK) under the Grant Number 123M656 and Middle East Technical University – Scientific Research Projects Coordination Unit under the Grant Number TEZ-D-310-2021-10665. The authors also thank the TUBITAK Directorate of Scientist Support Programs (BIDEB) for providing the scholarship.

References

1 N. Singh, A. Uppoor and D. G. Naik, Bone's smart envelope—The periosteum: Unleashing its regenerative potential for periodontal reconstruction, *Int. J. Contemp. Dent. Med. Rev.*, 2015, 090215, DOI: 10.15713/ins.ijcdmr.62.

2 E. J. Arnsdorf, L. M. Jones, D. R. Carter and C. R. Jacobs, The Periosteum as a Cellular Source for Functional Tissue Engineering, *Tissue Eng., Part A*, 2009, **15**(9), 2637–2642, DOI: 10.1089/ten.tea.2008.0244.

3 N. Li, J. Song, G. Zhu, X. Li, L. Liu, X. Shi and Y. Wang, Periosteum tissue engineering—A review, *Biomater. Sci.*, 2016, **4**(11), 1554–1561, DOI: 10.1039/C6BM00481D.

4 C. Colnot, X. Zhang and M. L. K. Tate, Current insights on the regenerative potential of the periosteum: Molecular, cellular, and endogenous engineering approaches, *J. Orthop. Res.*, 2012, **30**(12), 1869–1878, DOI: 10.1002/jor.22181.

5 W. Zhang, N. Wang, M. Yang, T. Sun, J. Zhang, Y. Zhao, N. Huo and Z. Li, Periosteum and development of the tissue-engineered periosteum for guided bone regeneration, *J. Orthop. Transl.*, 2022, **33**, 41–54, DOI: 10.1016/j.jot.2022.01.002.

6 R. R. Lorenz, M. E. Couch and B. B. Burkey, Head and Neck, in *Sabiston Textbook of Surgery*, ed. C. M. Townsend, R. D. Beauchamp, B. M. Evers and K. L. Mattox, Elsevier, 20th edn, 2017, pp. 796–797.

7 J. Li, D. He, L. Hu, S. Li, C. Zhang, X. Yin and Z. Zhang, Decellularized periosteum promotes guided bone regeneration via manipulation of macrophage polarization, *Biotechnol. J.*, 2023, **18**(10), 2300094, DOI: 10.1002/biot.202300094.

8 J. Chen, J. Chen, Z. Zhu, T. Sun, M. Liu, L. Lu, C. Zhou and B. Luo, Drug-Loaded and Anisotropic Wood-Derived Hydrogel Periosteum with Super Antibacterial, Anti-Inflammatory, and Osteogenic Activities, *ACS Appl. Mater. Interfaces*, 2022, **14**(45), 50485–50498, DOI: 10.1021/acsami.2c12147.

9 Z. Zhou, Y. Liu, W. Li, Z. Zhao, X. Xia, J. Liu, Y. Deng, Y. Wu, X. Pan, F. He, H. Yang, W. Lu, Y. Xu and X. Zhu, A Self-Adaptive Biomimetic Periosteum Employing Nitric Oxide Release for Augmenting Angiogenesis in Bone Defect Regeneration, *Adv. Healthcare Mater.*, 2024, **13**(3), 2302153, DOI: 10.1002/adhm.202302153.

10 A. Reizabal, C. M. Costa, L. Pérez-Álvarez, J. L. Vilas-Vilela and S. Lanceros-Méndez, Silk Fibroin as Sustainable Advanced Material: Material Properties and Characteristics, Processing, and Applications, *Adv. Funct. Mater.*, 2023, **33**(3), 2210764, DOI: 10.1002/adfm.202210764.

11 L. Yu, Q. Wei, J. Li, H. Wang, Q. Meng, E. Xie, Z. Li, K. Li, W. W. Shu, J. Wu, L. Yang, Y. Cai, F. Han and B. Li, Engineered periosteum-diaphysis substitutes with biomimetic structure and composition promote the repair of large segmental bone defects, *Composites, Part B*, 2023, **252**, 110505, DOI: 10.1016/j.compositesb.2023.110505.
12 K. Zhang and K. Cheng, Stem cell-derived exosome versus stem cell therapy, *Nat. Rev. Bioeng.*, 2023, **1**(9), 608–609, DOI: 10.1038/s44222-023-00064-2.
13 S. Zhu, Q. Zhang, X. Xu, Z. Liu, G. Cheng, D. Long, L. Cheng and F. Dai, Recent Advances in Silk Fibroin-Based Composites for Bone Repair Applications: A Review, *Polymers*, 2025, **17**(6), 772, DOI: 10.3390/polym17060772.
14 L. Deng, M. Hou, N. Lv, Q. Zhou, X. Hua, X. Hu, X. Ge, X. Zhu, Y. Xu, H. Yang, X. Chen, H. Liu and F. He, Melatonin-encapsuled silk fibroin electrospun nanofibers promote vascularized bone regeneration through regulation of osteogenesis-angiogenesis coupling, *Mater. Today Bio*, 2024, **25**, 100985, DOI: 10.1016/j.mtbio.2024.100985.
15 Ø. Arlov, F. L. Aachmann, A. Sundan, T. Espevik and G. Skjåk-Bræk, Heparin-Like Properties of Sulfated Alginates with Defined Sequences and Sulfation Degrees, *Biomacromolecules*, 2014, **15**(7), 2744–2750, DOI: 10.1021/bm500602w.
16 A. Vitiello and F. Ferrara, Low Molecular Weight Heparin, Anti-inflammatory/Immunoregulatory and Antiviral Effects, a Short Update, *Cardiovasc. Drugs Ther.*, 2023, **37**(2), 277–281, DOI: 10.1007/s10557-021-07251-6.
17 M. A. Gionet-Gonzales, R. C. H. Gresham, K. H. Griffin, A. Casella, R. P. Wohlgemuth, D. H. Ramos-Rodriguez, J. Lowen, L. R. Smith and J. K. Leach, Mesenchymal stromal cell spheroids in sulfated alginate enhance muscle regeneration, *Acta Biomater.*, 2023, **155**, 271–281, DOI: 10.1016/j.actbio.2022.10.054.
18 A. Kerschenmeyer, Ø. Arlov, V. Malheiro, M. Steinwachs, M. Rottmar, K. Maniura-Weber, G. Palazzolo and M. Zenobi-Wong, Anti-oxidant and immune-modulatory properties of sulfated alginate derivatives on human chondrocytes and macrophages, *Biomater. Sci.*, 2017, **5**(9), 1756–1765, DOI: 10.1039/C7BM00341B.
19 S. Gurung, D. Perocheau, L. Touramanidou and J. Baruteau, The exosome journey: From biogenesis to uptake and intracellular signalling, *Cell Commun. Signaling*, 2021, **19**(1), 47, DOI: 10.1186/s12964-021-00730-1.
20 Y. Yao, Y. Jiang, J. Song, R. Wang, Z. Li, L. Yang, W. Wu, L. Zhang and Q. Peng, Exosomes as Potential Functional Nanomaterials for Tissue Engineering, *Adv. Healthcare Mater.*, 2023, **12**(16), 2201989, DOI: 10.1002/adhm.202201989.
21 N. Su, C. Villicana and F. Yang, Immunomodulatory strategies for bone regeneration: A review from the perspective of disease types, *Biomaterials*, 2022, **286**, 121604.
22 S. Gupta, I. Qayoom, P. Gupta, A. Gupta, P. Singh, S. Singh and A. Kumar, Exosome-Functionalized, Drug-Laden Bone Substitute along with an Antioxidant Herbal Membrane for Bone and Periosteum Regeneration in Bone Sarcoma, *ACS Appl. Mater. Interfaces*, 2023, **15**(7), 8824–8839, DOI: 10.1021/acsami.2c18308.
23 W. Liang, H. Wu, L. Tan, X. Meng, W. Dang, M. Han, Y. Zhen, H. Chen, H. Bi and Y. An, Porcine pericardial decellularized matrix bilayer patch containing adipose stem cell-derived exosomes for the treatment of diabetic wounds, *Mater. Today Bio*, 2025, **30**, 101398, DOI: 10.1016/j.mtbio.2024.101398.
24 S. Mondal, S. Park, J. Choi, T. T. H. Vu, V. H. M. Doan, T. T. Vo, B. Lee and J. Oh, Hydroxyapatite: A journey from biomaterials to advanced functional materials, *Adv. Colloid Interface Sci.*, 2023, **321**, 103013, DOI: 10.1016/j.cis.2023.103013.
25 W. Gao, J. Deng, J. Ren, W. Zhang, Z. Wang, R. He, K. Wang, X. Shi and T. Liang, 3D-printed hydroxyapatite (HA) scaffolds combined with exos from BMSCs cultured in 3D HA scaffolds to repair bone defects, *Composites, Part B*, 2022, **247**, 110315, DOI: 10.1016/j.compositesb.2022.110315.
26 S. Akbaba, S. O. Turacli Karaguven, Z. Evis and A. Tezcaner, Boron and Zinc Co-doped Hydroxyapatites for Bone Tissue Engineering Applications, *Biol. Trace Elem. Res.*, 2025, **204**(3), 1417–1433, DOI: 10.1007/s12011-025-04756-1.
27 D. N. Rockwood, R. C. Preda, T. Yücel, X. Wang, M. L. Lovett and D. L. Kaplan, Materials fabrication from Bombyx mori silk fibroin, *Nat. Protoc.*, 2011, **6**(10), 1612–1631, DOI: 10.1038/nprot.2011.379.
28 H. Daemi, M. Mashayekhi and M. Pezeshki Modaress, Facile fabrication of sulfated alginate electrospun nanofibers, *Carbohydr. Polym.*, 2018, **198**, 481–485, DOI: 10.1016/j.carbpol.2018.06.105.
29 S. Akbaba, D. Atila, D. Keskin, T. Tezcaner and A. Tezcaner, Multilayer fibroin/chitosan oligosaccharide lactate and pullulan immunomodulatory patch for treatment of hernia and prevention of intraperitoneal adhesion, *Carbohydr. Polym.*, 2021, **265**, 118066, DOI: 10.1016/j.carbpol.2021.118066.
30 M. Taylor, A. J. Urquhart, M. Zelzer, M. C. Davies and M. R. Alexander, Picoliter Water Contact Angle Measurement on Polymers, *Langmuir*, 2007, **23**(13), 6875–6878, DOI: 10.1021/la070100j.
31 S. Wittaya-areekul and C. Prahsarn, Development and in vitro evaluation of chitosan–polysaccharides composite wound dressings, *Int. J. Pharm.*, 2006, **313**(1), 123–128, DOI: 10.1016/j.ijpharm.2006.01.027.
32 Y. You, B.-M. Min, S. J. Lee, T. S. Lee and W. H. Park, In vitro degradation behavior of electrospun polyglycolide, polylactide, and poly(lactide-*co*-glycolide), *J. Appl. Polym. Sci.*, 2005, **95**(2), 193–200, DOI: 10.1002/app.21116.
33 Y. D. Ladner, M. Alini and A. R. Armiento, The Dimethylmethylene Blue Assay (DMMB) for the Quantification of Sulfated Glycosaminoglycans, in *Cartilage Tissue Engineering*, ed. M. J. Stoddart, E. Della Bella and A. R. Armiento, Springer US, 2023, pp. 115–121, DOI: 10.1007/978-1-0716-2839-3_9.
34 D. Atila, D. Keskin and A. Tezcaner, Cellulose acetate based 3-dimensional electrospun scaffolds for skin tissue engineering applications, *Carbohydr. Polym.*, 2015, **133**, 251–261, DOI: 10.1016/j.carbpol.2015.06.109.
35 M. Zhu, S. Heydarkhan-Hagvall, M. Hedrick, P. Benhaim and P. Zuk, Manual Isolation of Adipose-derived Stem Cells

from Human Lipoaspirates, *JoVE*, 2013, **79**, e50585, DOI: 10.3791/50585.

36 Alexander Mildmay-White and Wasim Khan, Cell Surface Markers on Adipose-Derived Stem Cells: A Systematic Review, *Curr. Stem Cell Res. Ther.*, 2017, **12**(6), 484–492, DOI: 10.2174/1574888X11666160429122133.

37 D. W. Greening, R. Xu, H. Ji, B. J. Tauro and R. J. Simpson, A Protocol for Exosome Isolation and Characterization: Evaluation of Ultracentrifugation, Density-Gradient Separation, and Immunoaffinity Capture Methods, in *Proteomic Profiling: Methods and Protocols*, ed. A. Posch, Springer, New York, 2015, pp. 179–209, DOI: 10.1007/978-1-4939-2550-6_15.

38 E. Hosseini-Beheshti, W. Choi, L. B. Weiswald, G. Kharmate, M. Ghaffari, M. Roshan-Moniri, M. D. Hassona, L. Chan, M. Y. Chin, I. T. Tai and P. S. Rennie, Exosomes confer prosurvival signals to alter the phenotype of prostate cells in their surrounding environment, *Oncotarget*, 2016, **7**, 14639–14658, DOI: 10.18632/oncotarget.7052.

39 W.-J. Li, H. Chen, M.-L. Tong, J.-J. Niu, X.-Z. Zhu and L.-R. Lin, Comparison of the yield and purity of plasma exosomes extracted by ultracentrifugation, precipitation, and membrane-based approaches, *Open Chem.*, 2022, **20**(1), 182–191, DOI: 10.1515/chem-2022-0139.

40 A. E. Pazarçeviren, A. Tezcaner, D. Keskin, S. T. Kolukısa, S. Sürdem and Z. Evis, Boron-doped Biphasic Hydroxyapatite/β-Tricalcium Phosphate for Bone Tissue Engineering, *Biol. Trace Elem. Res.*, 2021, **199**(3), 968–980, DOI: 10.1007/s12011-020-02230-8.

41 U. Mayr-Wohlfart, J. Fiedler, K.-P. Günther, W. Puhl and S. Kessler, Proliferation and differentiation rates of a human osteoblast-like cell line (SaOS-2) in contact with different bone substitute materials, *J. Biomed. Mater. Res.*, 2001, **57**(1), 132–139, DOI: 10.1002/1097-4636(200110)57:1%253C132::AID-JBM1152%253E3.0.CO;2-K.

42 V. L. Singer, L. J. Jones, S. T. Yue and R. P. Haugland, Characterization of PicoGreen Reagent and Development of a Fluorescence-Based Solution Assay for Double-Stranded DNA Quantitation, *Anal. Biochem.*, 1997, **249**(2), 228–238, DOI: 10.1006/abio.1997.2177.

43 Y. He, H. Hara and G. Núñez, Mechanism and Regulation of NLRP3 Inflammasome Activation, *Trends Biochem. Sci.*, 2016, **41**(12), 1012–1021, DOI: 10.1016/j.tibs.2016.09.002.

44 A. Weber, P. Wasiliew and M. Kracht, Interleukin-1 (IL-1) Pathway, *Sci. Signaling*, 2010, **3**(105), 1–6, DOI: 10.1126/scisignal.3105cm1.

45 S. Mariathasan, D. S. Weiss, K. Newton, J. McBride, K. O'Rourke, M. Roose-Girma, W. P. Lee, Y. Weinrauch, D. M. Monack and V. M. Dixit, Cryopyrin activates the inflammasome in response to toxins and ATP, *Nature*, 2006, **440**(7081), 228–232, DOI: 10.1038/nature04515.

46 E. K. Park, H. S. Jung, H. I. Yang, M. C. Yoo, C. Kim and K. S. Kim, Optimized THP-1 differentiation is required for the detection of responses to weak stimuli, *Inflammation Res.*, 2007, **56**(1), 45–50, DOI: 10.1007/s00011-007-6115-5.

47 T. Murohara, T. Asahara, M. Silver, C. Bauters, H. Masuda, C. Kalka, M. Kearney, D. Chen, J. F. Symes, M. C. Fishman, P. L. Huang and J. M. Isner, Nitric oxide synthase modulates angiogenesis in response to tissue ischemia, *J. Clin. Investig.*, 1998, **101**(11), 2567–2578, DOI: 10.1172/JCI1560.

48 A. Rhimi, K. Zlaoui, K. Horchani-Naifer and D. J. Ennigrou, Characterization and extraction of sodium alginate from Tunisian algae: Synthesizing a cross-linked ultrafiltration membrane, *Iran. Polym. J.*, 2022, **31**(3), 367–382, DOI: 10.1007/s13726-021-01005-9.

49 S. Mohammadi, S. Ramakrishna, S. Laurent, M. A. Shokrgozar, D. Semnani, D. Sadeghi, S. Bonakdar and M. Akbari, Fabrication of Nanofibrous PVA/Alginate-Sulfate Substrates for Growth Factor Delivery, *J. Biomed. Mater. Res.-A*, 2019, **107**(2), 403–413, DOI: 10.1002/jbm.a.36552.

50 I. Freeman, A. Kedem and S. Cohen, The effect of sulfation of alginate hydrogels on the specific binding and controlled release of heparin-binding proteins, *Biomaterials*, 2008, **29**(22), 3260–3268, DOI: 10.1016/j.biomaterials.2008.04.025.

51 A. M. Syanda, V. I. Kringstad, S. J. I. Blackford, J. S. Kjesbu, S. S. Ng, L. Ma, F. Xiao, A. E. Coron, A. M. A. Rokstad, S. Modi, S. T. Rashid and B. L. Strand, Sulfated Alginate Reduces Pericapsular Fibrotic Overgrowth on Encapsulated cGMP-Compliant hPSC-Hepatocytes in Mice, *Front. Bioeng. Biotechnol.*, 2022, **9**, 816542, DOI: 10.3389/fbioe.2021.816542.

52 G. Pasternak, Y. Yang, B. B. Santos, F. Brunello, M. M. Hanczyc and A. Motta, Regenerated silk fibroin membranes as separators for transparent microbial fuel cells, *Bioelectrochemistry*, 2019, **126**, 146–155, DOI: 10.1016/j.bioelechem.2018.12.004.

53 H.-Y. Wang and Y.-Q. Zhang, Processing and characterisation of a novel electropolymerized silk fibroin hydrogel membrane, *Sci. Rep.*, 2014, **4**(1), 6182, DOI: 10.1038/srep06182.

54 C. Geão, A. R. Costa-Pinto, C. Cunha-Reis, V. P. Ribeiro, S. Vieira, J. M. Oliveira, R. L. Reis and A. L. Oliveira, Thermal annealed silk fibroin membranes for periodontal guided tissue regeneration, *J. Mater. Sci.: Mater. Med.*, 2019, **30**(2), 27, DOI: 10.1007/s10856-019-6225-y.

55 D. Lan, Z. Liu, J. Zhou, M. Xu, Z. Li and F. Dai, Preparation and characterization of silk fibroin/polyethylene oxide nanofiber membranes with antibacterial activity, *J. Biomed. Mater. Res.-A*, 2022, **110**(2), 287–297, DOI: 10.1002/jbm.a.37285.

56 E. Salimi, A. Ghaee, A. F. Ismail and M. Karimi, Antithrombogenicity and permeability of polyethersulfone hollow fiber membrane with sulfonated alginate toward blood purification, *Int. J. Biol. Macromol.*, 2018, **116**, 364–377, DOI: 10.1016/j.ijbiomac.2018.04.137.

57 T. W. Chen, S. J. Chang, G. C.-C. Niu, Y. T. Hsu and S. M. Kuo, Alginate-coated chitosan membrane for guided tissue regeneration, *J. Appl. Polym. Sci.*, 2006, **102**(5), 4528–4534, DOI: 10.1002/app.24945.

58 J. H. Aburabie, T. Puspasari and K.-V. Peinemann, Alginate-based membranes: Paving the way for green organic solvent nanofiltration, *J. Membr. Sci.*, 2020, **596**, 117615, DOI: 10.1016/j.memsci.2019.117615.

59 Y. Wang, N. Qin, C. Zhao, J. Yuan, S. Lu, W. Li, H. Xiang and H. Hao, The correlation between the methylation of PTEN gene and the apoptosis of osteosarcoma cells mediated by SeHA nanoparticles, *Colloids Surf., B*, 2019, **184**, 110499, DOI: 10.1016/j.colsurfb.2019.110499.
60 M. A. de Moraes and M. M. Beppu, Biocomposite membranes of sodium alginate and silk fibroin fibers for biomedical applications, *J. Appl. Polym. Sci.*, 2013, **130**(5), 3451–3457, DOI: 10.1002/app.39598.
61 Z. Luo, Q. Zhang, M. Shi, Y. Zhang, W. Tao and M. Li, Effect of Pore Size on the Biodegradation Rate of Silk Fibroin Scaffolds, *Adv. Mater. Sci. Eng.*, 2015, **2015**(1), 315397, DOI: 10.1155/2015/315397.
62 Z. Lin, A. Fateh, D. M. Salem and G. Intini, Periosteum: Biology and Applications in Craniofacial Bone Regeneration, *J. Dent. Res.*, 2014, **93**(2), 109–116, DOI: 10.1177/0022034513506445.
63 M. Daigneault, J. A. Preston, H. M. Marriott, M. K. B. Whyte and D. H. Dockrell, The Identification of Markers of Macrophage Differentiation in PMA-Stimulated THP-1 Cells and Monocyte-Derived Macrophages, *PLoS One*, 2010, **5**(1), e8668, DOI: 10.1371/journal.pone.0008668.
64 W. Chanput, J. Mes, R. A. M. Vreeburg, H. F. J. Savelkoul and H. J. Wichers, Transcription profiles of LPS-stimulated THP-1 monocytes and macrophages: A tool to study inflammation modulating effects of food-derived compounds, *Food Funct.*, 2010, **1**(3), 254–261, DOI: 10.1039/C0FO00113A.
65 H. Xing, R. Li, Y. Qing, B. Ying and Y. Qin, Biomaterial-based osteoimmunomodulatory strategies via the TLR4-NF-κB signaling pathway: A review, *Appl. Mater. Today*, 2021, **22**, 100969, DOI: 10.1016/j.apmt.2021.100969.
66 F. S. Sutterwala, S. Haasken and S. L. Cassel, Mechanism of NLRP3 inflammasome activation, *Ann. N. Y. Acad. Sci.*, 2014, **1319**(1), 82–95, DOI: 10.1111/nyas.12458.
67 H. M. Blevins, Y. Xu, S. Biby and S. Zhang, The NLRP3 Inflammasome Pathway: A Review of Mechanisms and Inhibitors for the Treatment of Inflammatory Diseases, *Front. Aging Neurosci.*, 2022, **14**, 879021, DOI: 10.3389/fnagi.2022.879021.
68 A. Motta, D. Maniglio, C. Migliaresi, H.-J. Kim, X. Wan, X. Hu and D. L. Kaplan, Silk Fibroin Processing and Thrombogenic Responses, *J. Biomater. Sci., Polym. Ed.*, 2009, **20**(13), 1875–1897, DOI: 10.1163/156856208X399936.
69 C. Huang, L. Dong, B. Zhao, S. Huang, Y. Lu, X. Zhang, X. Hu, Y. Huang, W. He, Y. Xu, W. Qian and G. Luo, Tunable Sulfated Alginate-based Hydrogel Platform with enhanced anti-inflammatory and antioxidant capacity for promoting burn wound repair, *J. Nanobiotechnol.*, 2023, **21**(1), 387, DOI: 10.1186/s12951-023-02144-2.
70 L. Kordelas, V. Rebmann, A.-K. Ludwig, S. Radtke, J. Ruesing, T. R. Doeppner, M. Epple, P. A. Horn, D. W. Beelen and B. Giebel, MSC-derived exosomes: A novel tool to treat therapy-refractory graft-versus-host disease, *Leukemia*, 2014, **28**(4), 970–973, DOI: 10.1038/leu.2014.41.
71 E. I. Yakubovich, A. G. Polischouk and V. I. Evtushenko, Principles and Problems of Exosome Isolation from Biological Fluids, *Biochemistry*, 2022, **16**(2), 115–126, DOI: 10.1134/S1990747822030096.
72 J. A. Welsh, D. C. I. Goberdhan, L. O'Driscoll, E. I. Buzas, C. Blenkiron, B. Bussolati, H. Cai, D. Di Vizio, T. A. P. Driedonks, U. Erdbrügger, J. M. Falcon-Perez, Q.-L. Fu, A. F. Hill, M. Lenassi, S. K. Lim, M. G. Mahoney, S. Mohanty, A. Möller, R. Nieuwland and K. W. Witwer, Minimal information for studies of extracellular vesicles (MISEV2023): From basic to advanced approaches, *J. Extracell. Vesicles*, 2024, **13**(2), e12404, DOI: 10.1002/jev2.12404.
73 X.-X. Li, L.-X. Yang, C. Wang, H. Li, D.-S. Shi and J. Wang, The Roles of Exosomal Proteins: Classification, Function, and Applications, *Int. J. Mol. Sci.*, 2023, **24**(4), 3061, DOI: 10.3390/ijms24043061.
74 B. Bhattacharya, R. Dhar, S. Mukherjee, S. Gorai, A. Devi, A. Krishnan, A. Alexiou and M. Papadakis, Exosome DNA: An untold story of cancer, *Clin. Transl. Discovery*, 2023, **3**(4), e218, DOI: 10.1002/ctd2.218.
75 S. R. Baglio, K. Rooijers, D. Koppers-Lalic, F. J. Verweij, M. Pérez Lanzón, N. Zini, B. Naaijkens, F. Perut, H. W. M. Niessen, N. Baldini and D. M. Pegtel, Human bone marrow- and adipose-mesenchymal stem cells secrete exosomes enriched in distinctive miRNA and tRNA species, *Stem Cell Res. Ther.*, 2015, **6**(1), 127, DOI: 10.1186/s13287-015-0116-z.
76 S. Kim, S. K. Lee, H. Kim and T. M. Kim, Exosomes Secreted from Induced Pluripotent Stem Cell-Derived Mesenchymal Stem Cells Accelerate Skin Cell Proliferation, *Int. J. Mol. Sci.*, 2018, **19**(10), 3119, DOI: 10.3390/ijms19103119.
77 D. H. Ha, S.-D. Kim, J. Lee, H. H. Kwon, G.-H. Park, S. H. Yang, J. Y. Jung, J. H. Lee, S. R. Park, J. Youn, S. H. Lee, J. E. Kim, J. Lim, H.-K. Lee, B. S. Cho and Y. W. Yi, Toxicological evaluation of exosomes derived from human adipose tissue-derived mesenchymal stem/stromal cells, *Regul. Toxicol. Pharmacol.*, 2020, **115**, 104686, DOI: 10.1016/j.yrtph.2020.104686.
78 A. Hunter, C. W. Archer, P. S. Walker and G. W. Blunn, Attachment and proliferation of osteoblasts and fibroblasts on biomaterials for orthopaedic use, *Biomaterials*, 1995, **16**(4), 287–295, DOI: 10.1016/0142-9612(95)93256-D.
79 J. Liu, B. D. Lawrence, A. Liu, I. R. Schwab, L. A. Oliveira and M. I. Rosenblatt, Silk Fibroin as a Biomaterial Substrate for Corneal Epithelial Cell Sheet Generation, *Invest Ophthalmol. Visual Sci.*, 2012, **53**(7), 4130–4138, DOI: 10.1167/iovs.12-9876.
80 C. Meng, Y. He, Z. Wei, Y. Lu, F. Du, G. Ou, N. Wang, X.-G. Luo, W. Ma, T.-C. Zhang and H. He, MRTF-A mediates the activation of COL1A1 expression stimulated by multiple signaling pathways in human breast cancer cells, *Biomed. Pharmacother.*, 2018, **104**, 718–728, DOI: 10.1016/j.biopha.2018.05.092.
81 A. Rutkovskiy, K.-O. Stensløkken and I. J. Vaage, Osteoblast Differentiation at a Glance, *Med. Sci. Monit. Basic Res.*, 2016, **22**, 95–106, DOI: 10.12659/MSMBR.901142.
82 Z. Tang, H. Chen, H. He and C. Ma, Assays for alkaline phosphatase activity: Progress and prospects, *TrAC, Trends Anal. Chem.*, 2019, **113**, 32–43, DOI: 10.1016/j.trac.2019.01.019.
83 B. Panilaitis, G. H. Altman, J. Chen, H.-J. Jin, V. Karageorgiou and D. L. Kaplan, Macrophage responses

to silk, *Biomaterials*, 2003, **24**(18), 3079–3085, DOI: 10.1016/S0142-9612(03)00158-3.

84 H. Yu, L. Lin, Z. Zhang, H. Zhang and H. Hu, Targeting NF-κB pathway for the therapy of diseases: Mechanism and clinical study, *Signal Transduction Targeted Ther.*, 2020, **5**(1), 209, DOI: 10.1038/s41392-020-00312-6.

85 M. Saraiva and A. O'Garra, The regulation of IL-10 production by immune cells, *Nat. Rev. Immunol.*, 2010, **10**(3), 170–181, DOI: 10.1038/nri2711.

86 D. Brough, P. Pelegrin and N. J. Rothwell, Pannexin-1-dependent caspase-1 activation and secretion of IL-1β is regulated by zinc, *Eur. J. Immunol.*, 2009, **39**(2), 352–358, DOI: 10.1002/eji.200838843.

87 T. T. Truong, V. H. M. Doan, D. Q. Nguyen, Q. D. Nguyen, J. Choi, B. Subramaniyan, J. Ahn, B. Lee, J. Oh and S. Mondal, Synergistic Therapeutic Effects of Prussian Blue Erbium-Doped Hydroxyapatite Nanoparticles in Photothermal Photodynamic Cancer Therapy, *ACS Biomater. Sci. Eng.*, 2025, **11**(5), 2639–2652, DOI: 10.1021/acsbiomaterials.5c00027.

88 W. Olejarz, G. Kubiak-Tomaszewska, A. Chrzanowska and T. Lorenc, Exosomes in Angiogenesis and Anti-angiogenic Therapy in Cancers, *Int. J. Mol. Sci.*, 2020, **21**(16), 5840, DOI: 10.3390/ijms21165840.

89 K. L. DeCicco-Skinner, G. H. Henry, C. Cataisson, T. Tabib, J. C. Gwilliam, N. J. Watson, E. M. Bullwinkle, L. Falkenburg, R. C. O'Neill, A. Morin and J. S. Wiest, Endothelial Cell Tube Formation Assay for the In Vitro Study of Angiogenesis, *JoVE*, 2014, **91**, e51312, DOI: 10.3791/51312.

